




Microstructure and Wear Behavior of MMC Coatings Deposited by Plasma Transferred Arc Welding and Thermal Flame Spraying Processes

A. Maslarevic¹  · G. M. Bakic² · M. B. Djukic² · B. Rajicic² · V. Maksimovic³ · V. Pavkov³

Received: 10 September 2019 / Accepted: 21 October 2019 / Published online: 31 October 2019
© The Indian Institute of Metals - IIM 2019

Abstract In this study, two erosion protection MMC coatings with WC particles were deposited by the plasma transferred arc (PTA) welding. One of the coatings with tungsten carbide WC in the NiBSi matrix (WC/NiBSi), and the second coating WC in NiCrBSi matrix (WC/NiCrBSi) was deposited by the flame spray process on the same substrate material S235JR steel. Experiments were performed using a gas blast sand erosion test facility with high-velocity erodent particles impact (approximately 100 m/s) at different particle impact angles (20°–45°), with an objective to study erosion wear characteristics and mass loss of two MMC coatings. Microstructural characterization of MMC coatings was done by scanning electron microscope equipped with energy-dispersive X-ray spectroscopy, whereas X-ray diffraction analysis was used for identification of present phases. The hardness of coatings was determined by Vickers hardness measurements. WC/NiBSi obtained by the PTA process shows superior hardness and erosion properties.

Keywords Erosion protection coatings · Plasma transferred arc (PTA) · Solid particle erosion · Wear · Impact angle · Particle velocity

1 Introduction

Erosion of surfaces by solid particles may cause a progressive loss of material, due to the mechanical interaction of particles carried by the working fluid stream. Due to its deleterious effect on the surface, erosive wear is a widespread type of wear, which may provoke within a very short time, a catastrophic failure and rapid collapse in the structural integrity of industrial parts and components. The erosion behavior of ductile materials differ from the behavior of brittle materials, especially from the aspect of an active erosion mechanism. The difference in behavior between these two groups of materials is most pronounced when compared to mass loss during erosive wear at different impact angles of erodent particles [1]. The maximum mass loss of brittle material is obtained when the impact angle of the erodent particles is $\sim 90^\circ$ [1], while the maximum mass loss of some ductile materials is approximately up to 45° of impact angle [2]. Factors that may influence erosion wear and the mass loss of the material are numerous, including properties of a target material, such as hardness, microstructure and surface properties. Also, in these processes, an important role is played by erodent particle characteristics, such as the morphology of erodent, angle of impingement, particle impact velocity, particle concentration in the fluid stream, as well as other factors such as nature of the carrier gas and its temperature [3–14].

The application of the hard surface erosion protection coatings on the base material is one of the techniques developed in order to reduce the damaging effects of erosive particles with the aim of extending the service life of industrial components exposed to severe erosion damages during operation [15]. A number of technologies have been developed for the application of erosion protective coatings; however, they all can be basically classified into

✉ A. Maslarevic
amaslarevic@mas.bg.ac.rs

¹ Innovation Center, Faculty of Mechanical Engineering, University of Belgrade, Kraljice Marije 16, Belgrade 11120, Serbia

² Faculty of Mechanical Engineering, University of Belgrade, Kraljice Marije 16, Belgrade 11120, Serbia

³ Vinca Institute of Nuclear Sciences, University of Belgrade, Belgrade 11001, Serbia

two major groups: the thermal spraying process and the weld overlay cladding—surfacing process. The most commonly used thermal spraying processes are flame spray (FS), wire arc spraying (AS), high-velocity oxygen-fuel (HVOF) thermal spray, detonation spray, plasma spray and cold spray. In addition to the conventional surfacing, welding processes such as gas tungsten arc welding (GTAW) and flux-cored arc welding (FCAW), also the plasma transferred arc (PTA) surfacing, are also widely used [16–21].

The PTA process is extensively used to deposit a variety of erosion-resistant coatings, including metal-matrix composite (MMC) coatings [22, 23], as well as metal coatings [24], and ceramic coatings [25], onto numerous substrate materials. According to previous studies of erosion resistance of different MMC coatings, it is evident that carbide particles embedded into the matrix as a reinforcement material directly affect the hardness, abrasion and erosion resistance, yielding excellent erosive wear resistance [26–28]. The structure and properties of the metal matrix have an important contribution to the preservation of erosion resistance of MMC coatings. For example, a softer and more ductile metal matrix has a higher impact resistance than a metal matrix with higher hardness and brittleness [29]. Among different particles as a reinforcing material, dispersed hard WC particles are mostly used for the fabrication of MMC coatings [27, 30, 31].

The aim of the present research is to study the influence of the impact of high-velocity/high-energy erodent particles and their impact angles on the erosive wear resistance behavior of two MMC erosion protection coatings, obtained by PTA and FS processes on the same substrate material. The experimental concept of this study has been significantly dictated by the industrial practice and usage of commonly and broadly used and commercially available WC/NiBSi and WC/NiCrBSi powders (EuTroLoy PG 6503 and Eutalloy PE 8902). These two specific coatings, with different chemical composition and carbide contents, obtained by PTA and FS processes, have significant industrial relevance for erosion protection of thermal power plant components exposed to very severe erosion conditions, i.e., high-velocity/high-energy erodent particles (100 m/s) [32].

2 Experimental Methods

2.1 Material and Procedure

Two different erosion protection coatings were deposited on the same substrate material, i.e., 100 × 100 × 10 mm plates of low-carbon steel S235JR (EN 10025). The first erosion protection coating was applied by the PTA

surfacing, i.e., a coating with tungsten carbide particles (WC) in the NiBSi matrix (denoted as WC/NiBSi). The second coating, WC in the NiCrBSi matrix (WC/CrNiBSi), was applied by the FS thermal spraying with post-heating treatment. The filler materials in the form of powder were used for both coating deposition processes. The chemical compositions of the substrate material and filler materials used in this study are given in Table 1. Both filler materials used in this study were commercially available powders produced by Castolin Eutectic Company. The trade name of the WC/NiBSi powder is EuTroLoy PG 6503, while the trade name of the WC/NiCrBSi powder is Eutalloy PE 8902. The metal matrix of both powders was obtained by the process of atomization. The W_2C/WC carbides in WC/NiBSi powder were manufactured by fusing and crushing. The WC carbides in WC/NiCrBSi powder were manufactured by the sintering process. The nominal particle size for WC/NiBSi powder is in the range of 63–180 μm , while in the case of WC/NiCrBSi powder it is in the range of 50–150 μm in accordance with the producer of powders.

Coatings were deposited by PTA using a device EuTronic Gap 3001 DC, while a CastoDyn 8000 device was used for FS. Both units were manufactured by Castolin Eutectic Company. The preparation of the substrate surface for the PTA coating was performed by grinding the surface in order to remove impurities and oxides. The surface grinding for PTA was done by an angular grinder. The used grinding wheel was made of regular aluminum oxide particles (abrasive grains) with the coarser grit size in a mesh (sieve size per inch: 14–36). The preparation of the substrate surface for the FS coating was done by blasting with Al_2O_3 particles (grit size: 106–150 μm). The PTA surfacing parameters and the FS spraying parameters are given in Table 2. The thicknesses of coatings deposited by PTA (WC/NiBSi) and by FS (WC/NiCrBSi) were approximately 3 mm and 1 mm, respectively. It should be noted that coatings deposited by FS were subjected to post-heating treatment after spraying. Post-heating treatment was applied by oxyacetylene torch.

2.2 Powder and Coating Characterization Methods

The characterization of both powders (WC/NiBSi, WC/NiCrBSi; see Table 1) was performed using a scanning electron microscope (SEM), type JEOL JSM 5800LV at different magnifications. Also, a backscatter electron (BSE) imaging technique was applied. X-ray diffraction (XRD) analysis of powders was performed using a Rigaku Ultima IV diffractometer, $CuK\alpha$ radiation ($\lambda = 1.54056\text{\AA}$). The scanning of samples was done through a range of 2θ diffraction angles (20° – 70°), with a step size of 0.02° . Phase identification of the data collected was performed by the program DiffracPlus using the database for XRD peak

Table 1 Chemical composition

Substrate material		Element (wt%)								
		C	Mn	P	S					
S235JR (EN 10025)		0.17	1.40	0.045	0.045					
Filler materials	Process	Element (wt%)								
		C	Cr	Ni	B	Si	Mn	Fe	Mo	WC
WC/NiBSi	PTA	0.1	0.20	Residue	2.47	3.47	–	0.69	–	60
WC/NiCrBSi	FS	0.83	15.6	Residue	3.29	4.25	–	4.0	–	35

Table 2 Surfacing parameters

Plasma transferred arc surfacing parameters	Filler material— powder (process) WC/NiBSi (PTA)
Welding current (A)	70
Arc voltage (V)	27.5
Powder feeding rate (g/min)	33
Plasma gas	Ar
Plasma gas flow rate (l/min)	2
Shield and carrier gas	95%Ar + 5%H ₂
Shield gas flow rate (l/min)	14
Carrier gas flow rate (l/min)	2.5
The speed of movement of the torch in the direction of the length of the sample (mm/s)	0.11
Oscillation velocity (mm/s)	7
Oscillation width (mm)	94
Oxyacetylene flame spraying parameters	Filler material— powder (process) WC/CrNiBSi (FS)
Oxygen pressure (bar)	4
Acetylene pressure (bar)	0.7
The distance of gun from the surface (mm)	150
Post-heating treatment temperature (°C)	1040

identification compiled by the Joint Committee on Powder Diffraction Standards (JCPDS).

Metallographic examination of all coatings and substrate was carried out by three different SEM units: JEOL JSM 5800LV, SEM FEI Inspect S50 and Tescan Vega 5130MM at different magnifications. The standard preparation process for SEM specimens was executed by cutting, grinding, polishing and etching (WC/NiBSi—3% solution nitric acid and ethyl alcohol—nital; WC/NiCrBSi—50 ml H₂O + 10 g CuSO₄ + 50 ml HCl). In order to identify the chemical composition of coatings, the semiquantitative energy-dispersive X-ray spectroscopy (EDS) was performed by the Bruker unit, coupled with FEI Inspect S50 SEM.

Vickers macrohardness (HV10: test load 10kgf, test duration 10 s) and microhardness (HV0.05: test load 50gf, test duration 15 s) measurements were carried out on the cross section of the sample by Buehler Identamet Microindentation Hardness Tester (model 1114) and Buehler Micromet 5101 testers, respectively. The mean values of five measurements are shown in this study.

2.3 Erosion Test

The major parameters affecting the erosion are the particle impact angle, the erodent particle velocity and the erodent concentration in the fluid stream [33]. Nowadays, numerous studies on erosion have been published, and the gas blast sand erosion test according to ASTM G76-07 standard has been typically used. However, in order to properly simulate very severe service conditions of some thermal power plant components, nonstandard erosion test was applied in this study. Actually, a very high erodent particle concentration and the particle impact velocities (~ 100 m/s) with the particle impact angle in the range of 20°–45° corresponding to the service condition [32] in the fluid stream were used. Some studies have already highlighted the importance of testing the erosion resistance of coatings with high-velocity particles (100 m/s), higher than those envisaged in the ASTM G76-07 standard [2, 34]. The narrow range of the particle impact velocities which has been used in this study (92, 100 and 109 m/s) is mainly conditioned by the results of experimental measurements for particle impact velocities in the industrial plant (90–110 m/s) [32].

Therefore, an experimental investigation was performed on a specially designed, in-house built, gas blast sand erosion test facility which was previously described [35]. Other researchers have already used similar gas blast sand erosion test facilities [36–38]. The erosion study was carried out at room temperature, while the effects of the particle velocity and impact angle on the mass loss were investigated under test conditions roughly corresponding to the real conditions during in situ exploitation of coatings [32]. Erosion tests were carried out using three different

Table 3 Erosion test parameters

Parameter	Value		
	Angular particle quartz (SiO ₂)		
Impact velocity—mean value (m/s)	92	100	109
Erodent particles impact angle (°)	20	20, 30, 45	20
Mean erodent granulation (mm)	0.33	0.33	0.33
Carrying gas	Air	Air	Air
Nozzle diameter (mm)	10	10	10
Distance between nozzle and sample (mm)	115	115	115
Erosion test duration (s)	120	120	120
Temperature (°C)	24	24	24
Feed particle rate (g/s)	50	50	50

particle velocities (92, 100 and 109 m/s) and for three erodent particle impact angles (20°, 30° and 45°). A total of three samples of each type of coating were tested under each experimental erosion condition. All erosion test parameters are shown in Table 3.

The mass was measured before and after the erosion test in order to determine the mass loss of the eroded samples. The mass was measured by analytical balance, precision 0.1 g, produced by E. Mettler.

2.3.1 Particle Velocity Determination

The particle impact velocity is a function of the back pressure used on the gas blast sand erosion test unit. A double-disk method was used in order to measure particle impact velocity for different used pressures [39]. Calculated mean values for the particle velocities based on the double-disk method were 92, 100 and 109 m/s for pressures 3, 4 and 5 bar, respectively, as shown in Table 3, together with other relevant parameters of the erosion test.

3 Results and Discussion

3.1 Powder Characterization

SEM micrographs of the morphology of powders, used as a filler material during coating deposition process, are shown in Figs. 1a–d. The X-ray diffraction patterns of WC/NiBSi and WC/NiCrBSi powders in their initial condition (see Table 1) are shown in Fig. 1e, f, respectively.

The morphology of powder filler materials clearly indicates the presence of a carbide phase with the irregular shape and the metallic phase with the spherical shape (Fig. 1a–d). The XRD analysis of WC/NiBSi and WC/NiCrBSi powders shows that there is a difference in chemical compositions of carbides in these two powders

(see Fig. 1e, f). In WC/NiBSi powder, WC and W₂C carbide types are detected, while in WC/NiCrBSi powder only WC carbide is detected, which is a consequence of powder manufacturing.

During the processing of fused W₂C/WC carbides for PTA WC/NiBSi powder, the goal is to achieve as higher content of WC carbide as possible in the W₂C/WC mixture, because of better tribological resistance of WC [40]. When the carbon content is about 3.7–4.1 wt%, WC phases in conventional hardfacing are typically eutectoid W₂C/WC particles—carbides [22] which are prone to high-temperature dissolution. Also, W₂C carbide is less desirable due to its high brittleness and susceptibility to dissolution during welding. A mixture with sufficient content of carbon is rapidly cooled during powder manufacturing and then crushed, forming angular shape, as shown in Fig. 1a, c. Unlike WC in WC/NiBSi powder (PTA), WC in WC/NiCrBSi powder (FS) is obtained by the sintering process, resulting in the porous structure of carbides (Fig. 1b, d (highlighted with arrows)).

Due to different contents of alloying elements (C, Cr, B, Si, and Fe), these atomized spherical particles form different matrix and intermetallic/metalloid compounds [41–43]. The metal matrix of both powders (content: WC/NiBSi ~ 40 wt% and WC/NiCrBSi ~ 65 wt%) is obtained by the process of atomization, which is characterized by the spherical shape of particles.

3.2 Microstructure of Coatings

SEM micrographs of the microstructure of certain areas of both coatings and EDS measurement points (marked with numbers in yellow and red) are shown in Figs. 2, 3 and 4, while EDS analysis for different measurement points presented in Figs. 2, 3 and 4 are shown in Tables 4, 5 and 6.

The microstructure of the WC/NiBSi (PTA) coating is shown in Fig. 2, whereas the area of the same coating matrix in the vicinity of the eutectoid W₂C/WC carbide is shown in Fig. 3. Unlike carbides and other phases with high hardness formed during the deposition/solidification process, in this case, WC carbide has been added prior to manufacturing. Figure 2a shows a coating of the WC/NiBSi (PTA), i.e., a multi-phase matrix in the vicinity of the WC. The multi-phase matrix consists of three characteristic phases indicated by 1–3 in Fig. 2b.

The chemical composition of the WC/NiBSi (PTA) coating obtained at different EDS measurement points shown in Figs. 2b and 3 is presented in Tables 4 and 5. It is important to note that data for carbon contents shown in Tables 4, 5 and 6 are not reliable due to a limitation of used conventional SEM and EDS X-ray types of equipment. Specifically, EDS microanalysis is not accurate for low atomic number elements, such as C, B, N and O, while in

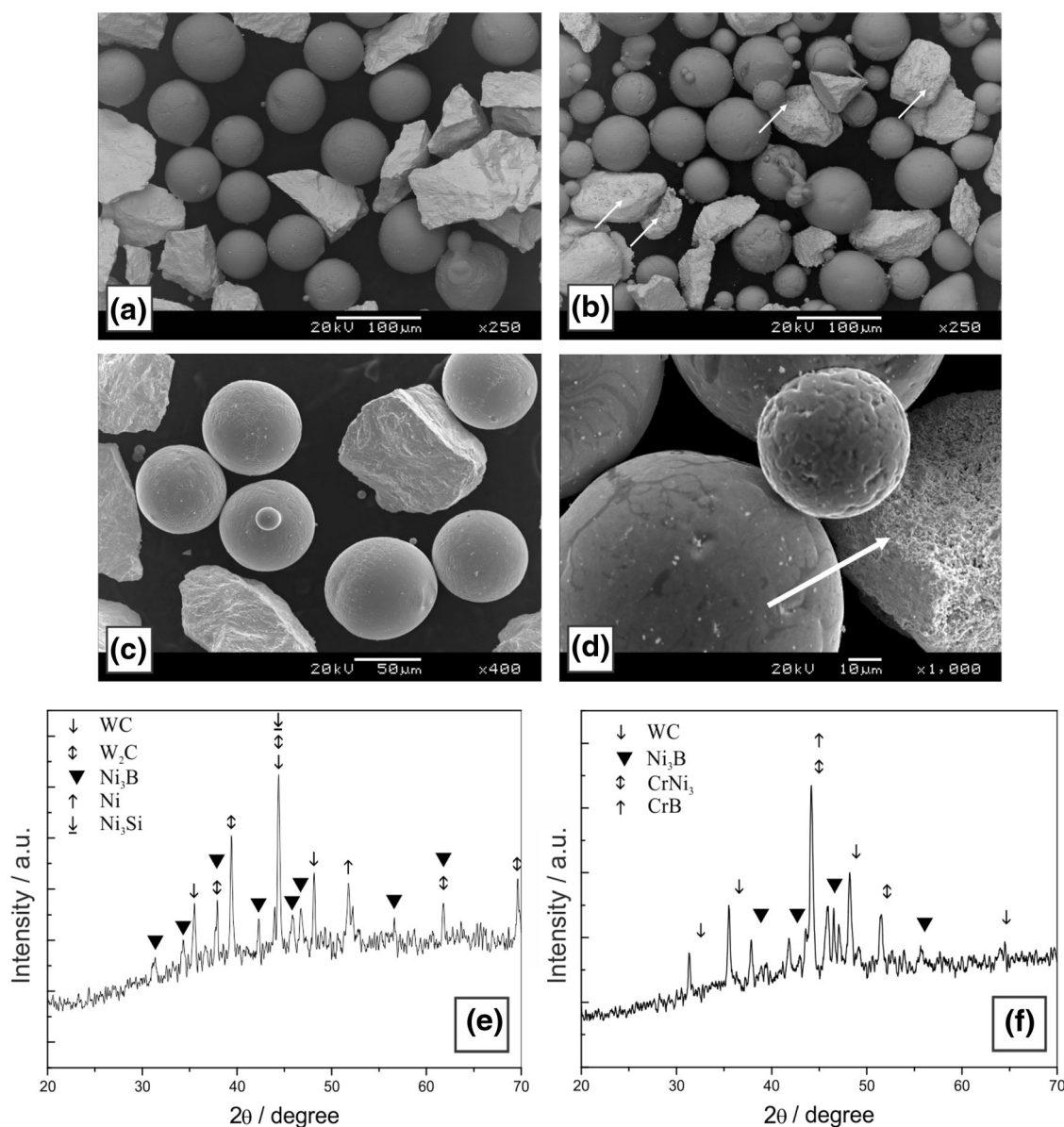


Fig. 1 SEM/XRD of the powders: **a** micrograph WC/NiBSi—BSE; **b** micrograph WC/NiCrBSi—BSE; **c** micrograph WC/NiBSi; **d** micrograph WC/NiCrBSi; **e** WC/NiBSi—XRD; **f** WC/NiCrBSi—XRD

the new EDS systems, this detection efficiency is improved. Nevertheless, it is not recommended as a technique for quantifying very low atomic number elements like carbon [44, 45].

Both phases 1 and 2 contain W, Ni, Fe, Cr, Si and C, as determined by EDS analysis and are shown in Table 4, points 1 and 2. According to the literature [46], B is bound with Ni forming Ni_3B . EDS results show that in phases 1 and 2 of the NiBSi matrix (Table 4, points 1 and 2), the presence of W is detected (phase 1: W = 3.52% and phase 2: W = 13.33%), although it has not been added in the original powder. This fact clearly indicates that during PTA deposition, the process of partial decomposition of W_2C /WC has taken place. Phases 1 and 2 (Table 4, points 1 and

2) can be characterized as interdendritic zones, which, according to the literature [22, 47], consist of secondary carbides, nickel boride (Ni_3B) and silicides, while phase 3 (Table 4, point 3) consists of primary γ -Ni solid solution. A slightly higher Fe content in all three phases may be ascribed to the dilution effect when Fe from a substrate is mostly dissolved in γ -Ni. Similar observations have also been confirmed by other researchers [22, 47].

The main disadvantage of WC carbides in carbide-reinforced MMC coatings is that, due to its relatively low temperature of formation, in comparison with the very high temperature of the PTA process, arc which reaches temperatures as high as 33,000 °C [48], may be easily dissolved in the matrix phase during deposition [49, 50] when

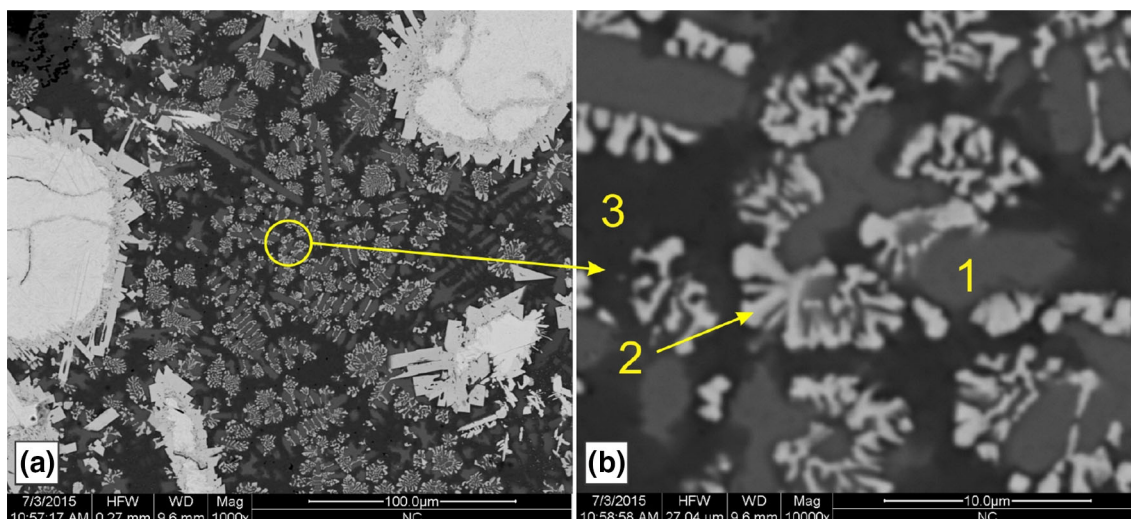


Fig. 2 SEM of the WC/NiBSi (PTA): **a** micrograph, WC/NiBSi; **b** detail from **a**, matrix, magnification $\times 10,000$ (1–3, three characteristic phases and corresponding EDS measurement points, see Table 4)

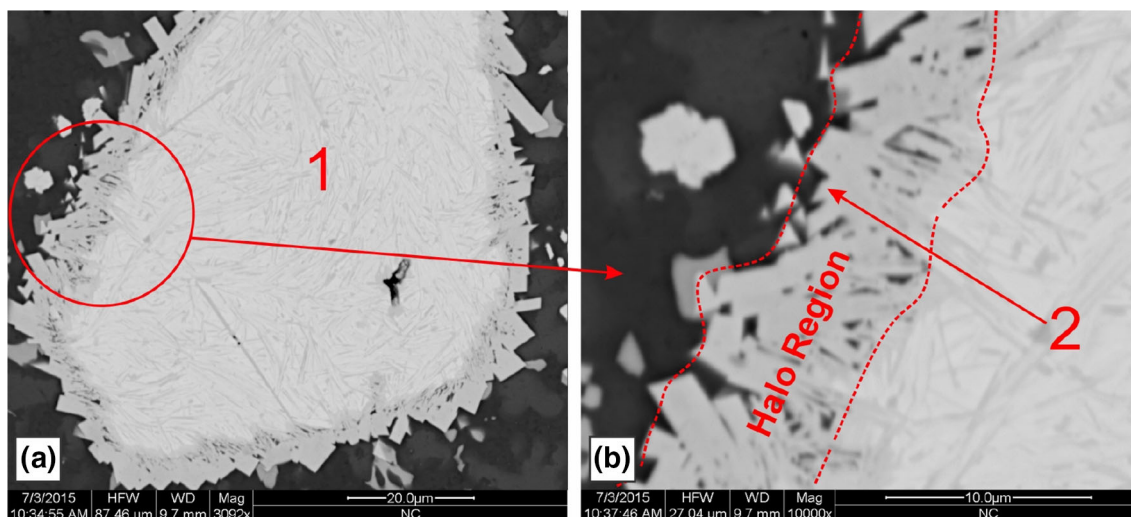


Fig. 3 SEM of the WC/NiBSi (PTA): **a** micrograph, eutectoid W_2C/WC carbide; **b** detail from **a**, magnification $\times 10,000$; (1–2, two characteristic phases, zone 1 from **a**, eutectoid W_2C/WC carbide, zone 2 from **b**, halo region and corresponding EDS measurement points, see Table 5)

excessive arc current provides sufficient heat [30]. The process of dilution of the substrate material also influences the properties of coating in the vicinity of the substrate. The enriched matrix has an effect on the decrease in wear-resistant properties of the coating [22]. This effect can be minimized when deposition of the metal is performed with the minimum possible heat input during the deposition process [22]. As can be seen in Fig. 3a, the primary W_2C/WC is partially decomposed during the formation of the coating and, as a result, along the edges of the primary carbide, a halo region is formed with visible effects of decomposition (Fig. 3b). The partial decomposition of the primary carbide during the deposition process is also

confirmed by the increase in the Ni content in the boundary zone W_2C/WC —matrix (Table 5, points 1 and 2), detected particularly in the halo region marked as zone 2 in Fig. 3b (Ni = 2.84%) [51, 52]. Eutectoid W_2C/WC carbides are typically distinguished from other types of carbides by the presence of alternating W_2C and WC lamellae in the microstructure [22]. In Fig. 3b, the needlelike lamellar microstructure can be observed, most likely consisting of WC carbide lamellas (darker lamellas) and W_2C carbide lamellas (lighter lamellas). Also, in the halo region, there are sharp WC carbides (dark colored), which can be identified on the basis of the distinguished differences in color of the lighter colored middle part of the observed

Fig. 4 SEM of the WC/NiCrBSi (FS): **a** micrograph, WC/NiCrBSi; **b** substrate-coating, EDS line profile; (1–2, two characteristic phases, zones 1—the WC carbide and 2—the nickel binder region from **a** and corresponding EDS measurement points, see Table 6)

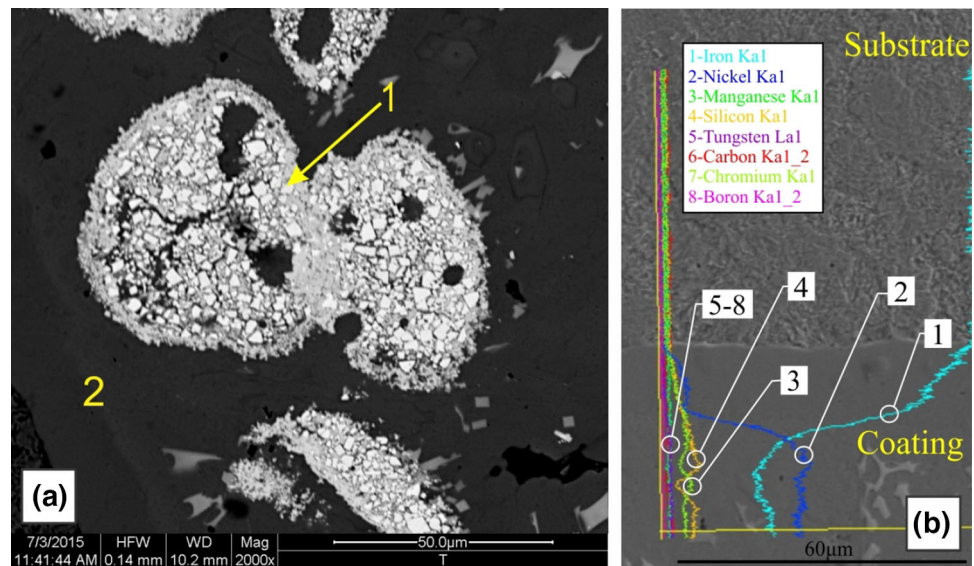


Table 4 Chemical composition of the WC/NiBSi (PTA), EDS points shown in Fig. 2b

EDS points	Element (wt%)					
	C	Cr	Ni	Si	Fe	W
Point 1	6.01	0.29	74.93	1.95	13.30	3.52
Point 2	8.53	0.28	62.48	2.17	12.77	13.77
Point 3	5.66	–	83.1	1.61	9.63	–

Table 5 Chemical composition of the WC/NiBSi (PTA), EDS points shown in Fig. 3

EDS points	Element (wt%)			
	C	Ni	Fe	W
Point 1	6.50	0.13	–	93.37
Point 2	10.85	2.84	1.24	85.07

Table 6 Chemical composition of the WC/NiCrBSi (FS), EDS points shown in Fig. 4a

EDS points	Element (wt%)					
	C	Cr	Ni	Si	Fe	W
Point 1	8.15	–	2.16	0.81	1.22	87.66
Point 2	3.54	4.80	67.63	1.58	22.45	–

carbide phase, which consists of W_2C and WC carbides [51, 52].

SEM micrographs of the microstructure of the WC/NiCrBSi (FS) coating and the substrate-coating zone together with the EDS line profile are shown in Fig. 4a, b. The chemical composition of the WC/NiCrBSi (FS)

coating obtained at different EDS measurement points shown in Fig. 4a is presented in Table 6.

The EDS analysis of sintered carbide (Table 6, point 1) shows that they are mainly composed of W-based carbide ($W = 87.66\%$), while the content of other elements is in accordance with the initial chemical composition of the powder. During the formation of a flame spray MMC coating using WC/NiCrBSi powders, the highest hardness and other wear resistance properties are obtained with WC content of approximately 35 wt%. Further increase in WC content will lead to higher porosity and consequently decrease in the mechanical properties [53]. The process of sintering used for the production of carbides in WC/NiCrBSi powder results in a porous structure of carbides (WC-type), as shown in Fig. 4a (zone 1), compared with denser carbides (W_2C /WC-type) in a coating obtained by the fusing process (see Fig. 3a).

The Ni binder region is present in the immediate vicinity of the substrate (Fig. 4a—zone 2 and Table 6, point 2). In addition to the Ni binder region, other authors have also identified chromium carbides and nickel borides in coatings with a similar chemical composition [46, 54]. Also, the coating matrix in the substrate-coating zone is enriched by a higher amount of Fe diffusing from the substrate, during subsequent heating of a coating (Fig. 4b). Similar results for NiCrBSi (FS) coating have also been obtained by other authors [55].

3.3 Hardness Measurements

Microhardness of both coatings was measured perpendicular to the substrate-coating bonding layer. SEM micrographs show the characteristic zones in which the test was carried out (Fig. 5). The obtained values for the base metal

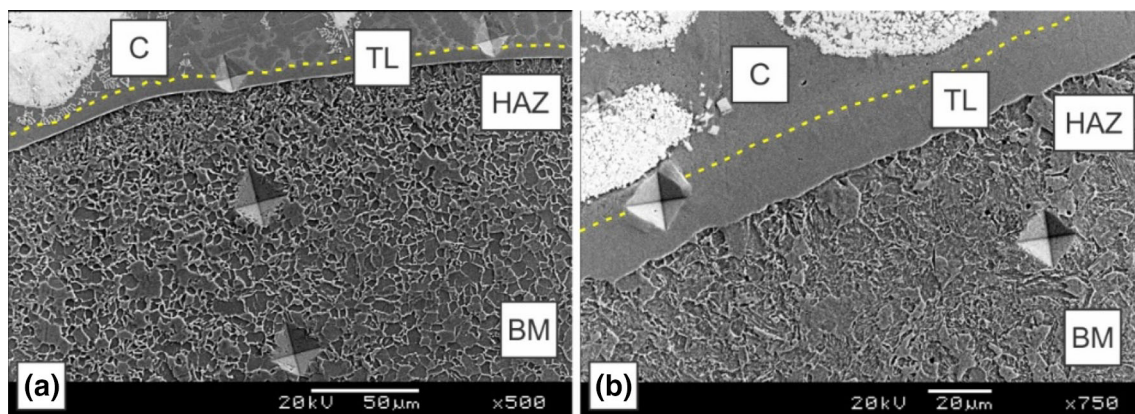


Fig. 5 SEM, microhardness measuring positions: **a** WC/NiBSi (PTA) and **b** WC/NiCrBSi (FS)

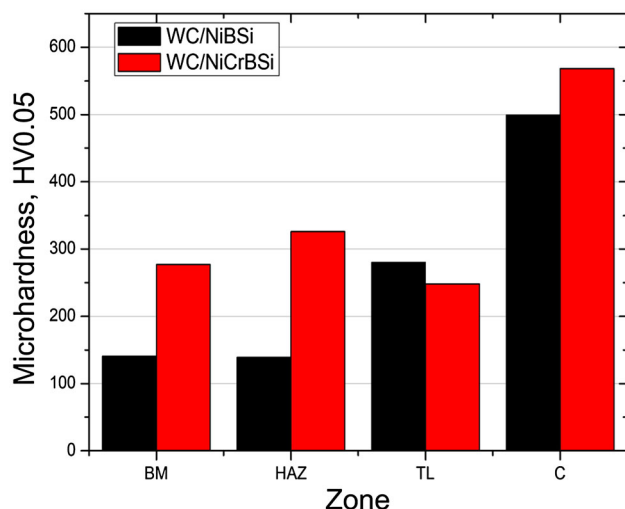


Fig. 6 Microhardness values of both coatings: WC/NiBSi (PTA) and WC/NiCrBSi (FS) in different zones of base metal (BM), heat-affected zone (HAZ), transition layer (TL) and coating matrix (C)

(BM), heat-affected zone (HAZ), transition layer (TL) and coating matrix (C) are shown in Fig. 6. Also, the hardness of carbide phases was measured.

The microhardness measurements of different carbides detected by SEM in both coatings (WC/NiBSi and WC/NiCrBSi) reveal that the hardness of W_2C/WC in WC/NiBSi (PTA) coating is in the 1171–1892 HV0.05 range (mean value 1664 ± 293 HV0.05). This value is higher than the microhardness of WC in WC/NiCrBSi (FS) coating, which is in the 857–1049 HV0.05 range (mean value 940 ± 91 HV0.05) (compare Fig. 5a vs. 5b). This is not surprising bearing in mind the fact that WC in the WC/NiBSi coating is much harder and has a denser structure (see Fig. 3a) compared with WC in the WC/NiCrBSi coating (see Fig. 4a). The hardness of carbide phases in MMC coatings is an important factor in erosion resistance. Higher hardness of carbides and a more ductile matrix of

MMC coating are beneficial for the prevention of both cutting and cracking mechanisms of erosion [56].

In Fig. 6, it is possible to notice a change in microhardness in different base metal/coating zones. The microhardness of a coating deposited by FS (WC/NiCrBSi) is substantially higher over the entire base material thickness (BM and HAZ) of the sample, which is a direct consequence of the post-heating treatment of the coating after its deposition (post-heating temperature: 1040 °C, Table 2) and small sample thickness. For both coatings, it can be noticed that the microhardness values in the transition layer (TL) are lower than in the coating matrix (C), mainly due to the absence of carbides in the TL zone for both coatings (see Figs. 2, 3 and 4).

The hardness of carbide phases in MMC coatings together with other hardness-based parameters is important factors in erosion resistance. One of these factors is the hardness ratio, which takes into account the ratio between macrohardness and microhardness of coating matrix (macrohardness/microhardness matrix ratio: $HV10/HV0.05_{Matrix}$) (Table 7).

The macrohardness/microhardness matrix ratio ($HV10/HV0.05_{Matrix}$) may be considered as one of the possible indicators of the erosion resistance of MMC coatings. However, many additional experiments are needed in order to confirm the universality and possibilities for the broader applicability of this indicator outside of the parameters used in this particular erosion experiment of MMC

Table 7 Macrohardness of coatings, microhardness of matrix and its ratio

Coating (process)	HV10 _{mean}	HV0.05 _{mean, Matrix}	HV10/HV0.05 _{Matrix}
WC/NiBSi (PTA)	711 ± 7	449 ± 55	1.42
WC/NiCrBSi (FS)	624 ± 18	568 ± 128	1.1

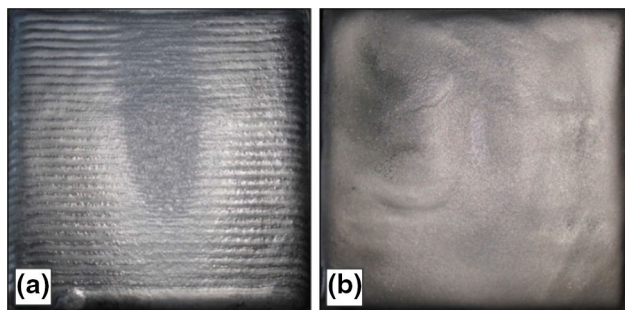


Fig. 7 Macroimages of MMC coatings eroded at 100 m/s (erodent particle impact angle: $\alpha = 20^\circ$): **a** WC/NiBSi (PTA); **b** WC/NiCrBSi (FS)

coatings. It is important to note that the difference in carbide contents in the PTA and FS coatings, and the other important microstructural factors—indicators, should be also taken into account in order to comprehensively compare the erosion resistance of different MMC coatings. These factors are the volume fraction of original carbides, the sizes of the carbides and their distribution.

According to the data shown in Table 7, it can be concluded that the contribution of carbides to the hardness values of coating deposited by PTA (WC/NiBSi (PTA): $HV_{10}/HV_{0.05_{Matrix}} = 1.42$) is higher than the hardness of coating sprayed by FS (WC/NiCrBSi (FS): $HV_{10}/HV_{0.05_{Matrix}} = 1.1$). This means that despite the fact that hard WC particles have been introduced into the matrix, their contribution to the increase in hardness is greatly reduced by other factors of which the most dominant is the porosity of oxyacetylene flame sprayed (FS) coating (see Fig. 4a). The porosity of coatings deposited by FS is significantly higher than coatings deposited by PTA, due to the very nature of the processes (spraying and surfacing). Despite the fact that it is expected to detect a generally lower porosity content in FS coating after post-heat

treatment at $\sim 1000^\circ\text{C}$, the SEM micrographs of both coatings at lower magnifications, which are not shown here, have confirmed higher porosity level in the FS coating.

3.4 Erosion Test

The visual inspection and macrophotography of eroded coating surfaces were done for all erosion tested samples. It is observed how the shape of the eroded zone changes with different erodent particle impact angles and different erodent particle velocities. Significant differences in the shape of the damaged zones are not observed for different erodent particle velocities, while for different impact angles, these differences are clearly visible and similar for all coatings. An example of similar shape of the damaged zone for different coatings (WC/NiBSi—PTA and WC/NiCrBSi—FS) eroded at 100 m/s and 20° impact angle is shown in Fig. 7.

Erosion test results, i.e., mass loss as a function of erodent particle impact velocity and as a function of erodent particle impact angle, are shown in Figs. 8a, b, respectively.

Comparison of erosion test results of WC/NiBSi (PTA) and WC/NiCrBSi (FS) coatings clearly indicates the difference in erosion resistance due to different morphology of the matrix and carbides: More compact shape of carbide particles (see Fig. 2b and Fig. 3a) and the softer matrix of the WC/NiBSi (PTA) coating ($HV_{0.05_{mean, Matrix}} = 449 \pm 55$, see Table 7) provide a higher erosion resistance.

The mass loss is functionally dependent on the erodent particle impact velocity, and mass loss increases with an increase in the impact velocity (Fig. 8a). However, the WC/NiCrBSi (FS) coating has lower erosion resistance (erodent particle impact angle: $\alpha = 20^\circ$) for all three impact velocities ($V = 92, 100$ and 109 m/s) than WC/NiBSi

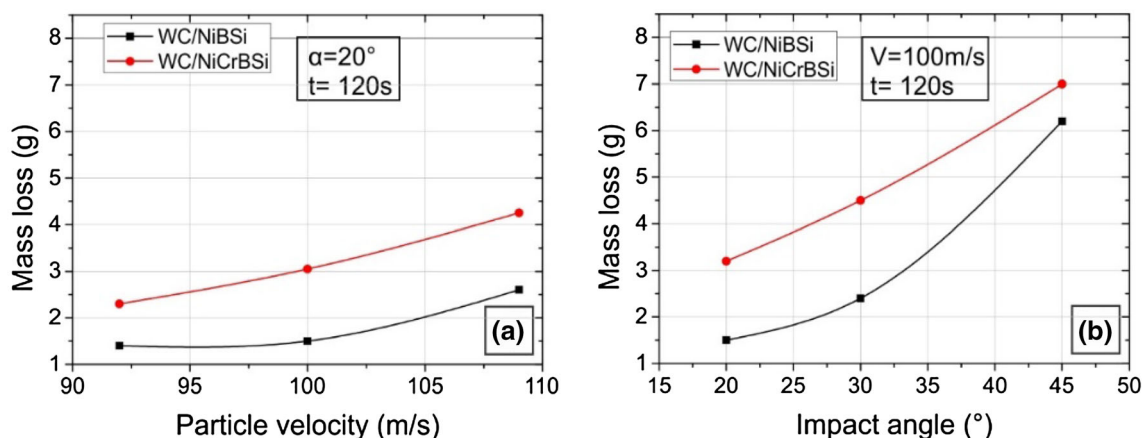


Fig. 8 Erosion test—mass loss of two coatings WC/NiBSi (PTA) and WC/NiCrBSi (FS): **a** as a function of erodent particle impact velocity (erodent particle impact angle: $\alpha = 20^\circ$); **b** as a function of erodent particle impact angle (erodent particle impact velocity: $V = 100$ m/s)

(PTA) coating. These data clearly indicate that surfaces exposed to the high-velocity erosion are better protected by the WC/NiBSi (PTA) coating than by the WC/NiCrBSi (FS) coating deposited by FS (Fig. 8a).

Generally, with an increase in the particle impact angle, mass loss of both tested coatings increases (Fig. 8b). However, the WC/NiCrBSi (FS) coating has lower erosion resistance for all three impact angles ($\alpha = 20^\circ, 30^\circ$ and 45°) than WC/NiBSi (PTA) coating.

All these results indicate that coating WC/NiBSi obtained by the PTA process shows superior hardness and erosion properties compared to WC/NiCrBSi sprayed by the FS process.

3.5 Erosion Mechanism

Erosion mechanisms were analyzed on samples exposed to the highest particle velocity (109 m/s) and the lowest impact angle (20°). Since WC/NiBSi (PTA) coating

belongs to the MMC materials, matrix and carbides are not eroded by the same mechanisms. The matrix material removal was done mainly by scratching and rubbings, as shown by the ductile scratching and rubbing traces on the surface (Fig. 9a, b). Also, the matrix was eroded by the mechanism of the cutting (Fig. 9b).

Being very hard and brittle, carbide particles are eroded as brittle materials. The maximum mass loss of brittle material is obtained when the impact angle of the erodent particles is $\sim 90^\circ$ [1], while with decreasing impact angle, mass loss of material becomes lower.

During erosion of the MMC coating, the softer matrix around the carbide phase is first eroded and the fraction of carbide particles remains above the matrix surface (Figs. 9a–c). In this case, the surface of the carbides above the surface of the eroded matrix is no longer exposed to erosion with an impact angle of 20° . Namely, the impact angle increases up to $\sim 90^\circ$, which is unfavorable for brittle materials. Although the erodent particles have a

Fig. 9 SEM micrographs showing the eroded surface morphology of WC/NiBSi (PTA) coating: **a, b** cross section; **c, d** topographical images

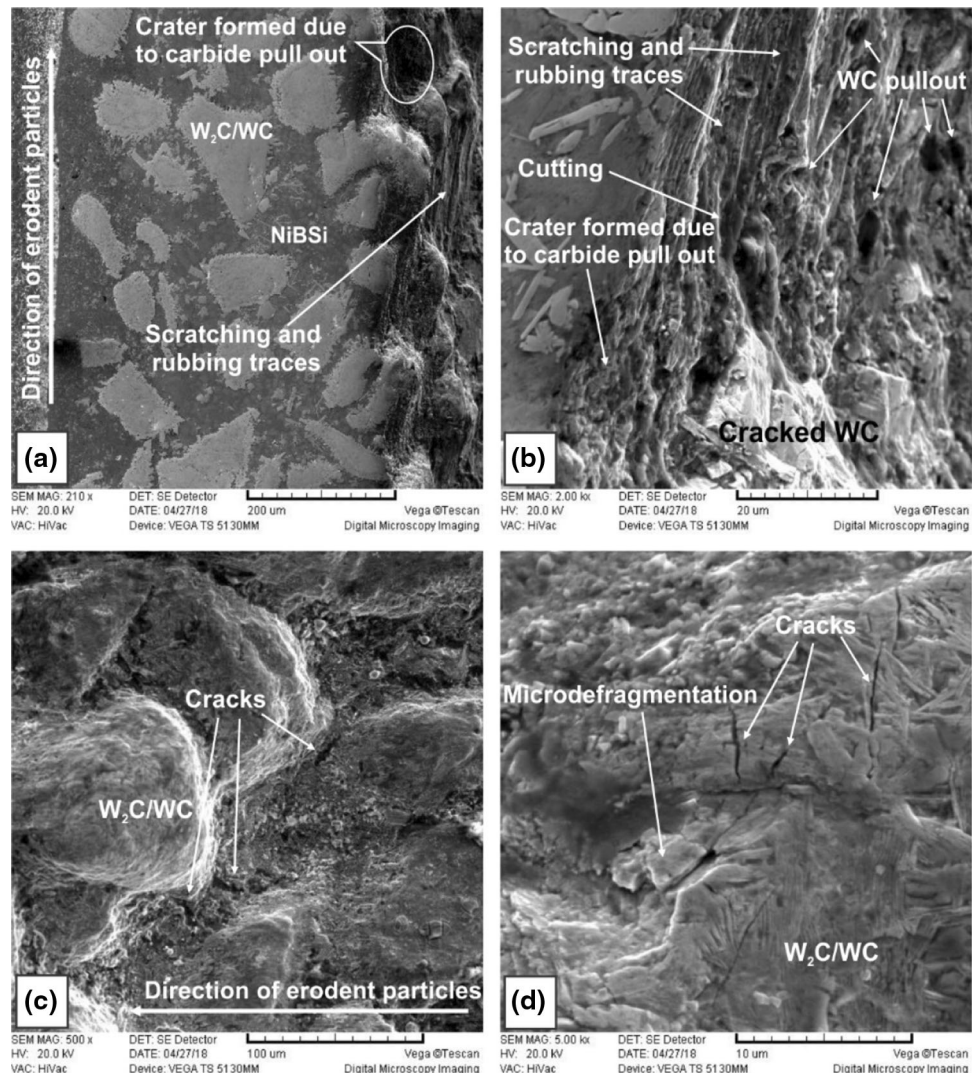
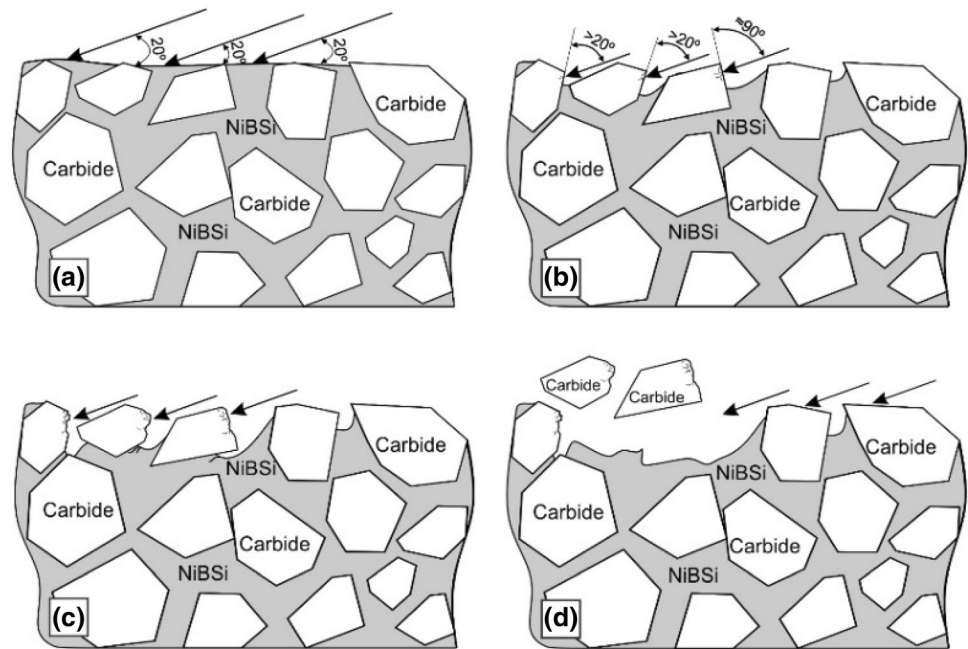


Fig. 10 Schematic display of erosion mechanism in WC/NiBSi (PTA) coating



lower value of hardness than the carbide particles, during rubbing they still have high kinetic energy. Therefore, the erodent particles initiate cracks and microdefragmentation on carbides surfaces (Fig. 9d). Also, cracks are observed at the interface between the matrix and carbides as a result of erodent particle impact during erosion. During the erosion process, carbides lose contact with matrix by the formation of cracks caused by the action of shear loads (Fig. 9c). Figure 10 schematically shows the eroding mechanism of WC/NiBSi (PTA) coating.

Figure 11 shows an eroded WC/NiCrBSi coating. The matrix removal was mainly done by cutting with the presence of plastic deformation and lips (Figs. 11c, d), with carbides, partially pulled out (Fig. 11b). Figure 12 schematically shows the eroding mechanism of WC/NiCrBSi (FS) coating.

The erosion resistance of this coating is achieved by the process of accumulation of carbide particles representing a barrier for sliding erodent particles. During the impact, only individual carbide particles are ejected from the surface (Figs. 11b, d and 12d, e). The erodent particles do not continue to slip after impact, as most of the energy is lost during penetration into the material in the vicinity of the carbides that are pulled from the matrix, and then completely lose energy when they impact on the next carbide.

The weak joint between WC particles and matrix during erosion has a great impact on the reduction of erosion resistance of the FS coatings. Similar conclusion for the WC/NiCrBSi coating deposited by the FS process was also detected by Rodríguez et al. [57].

4 Conclusions

The effects of different particle velocities and impact angles on erosion behavior of two metal-matrix composite (MMC) coatings have been investigated. WC/NiBSi coating was processed by plasma transferred arc (PTA) deposition, whereas oxyacetylene flame spraying (FS) was used for WC/NiCrBSi coating deposition. In all cases, plates of low-carbon steel S235JR (EN 10025) served as a substrate. The main conclusions on the erosion behavior of these coatings are as follows:

- WC/NiBSi coating obtained by the PTA process shows superior hardness and erosion properties. The main reasons for such a behavior are the composition, morphology and the production process of WC dispersed as a reinforcing material in the metal matrix of MMC coatings, a significantly smaller porosity, and a much more ductile metal matrix of coatings deposited by the PTA process, which together contribute to the increase in the erosion resistance. Also, the porosity level strongly depends on the process parameters (heat input, shielding, etc.), but generally, the level of porosity obtained by the PTA process is typically lower than those obtained by the FS process.
- WC/NiBSi coating (PTA) gets eroded by several solid particle erosion mechanisms. The matrix material gets eroded mainly by scratching, rubbings and cutting, while carbide particles are eroded by the initiation of cracks and micro defragmentation.
- The matrix material of the coating WC/NiCrBSi (FS) gets eroded mainly by cutting with the presence of

Fig. 12 Schematic display of erosion mechanism in WC/NiCrBSi (FS) coating

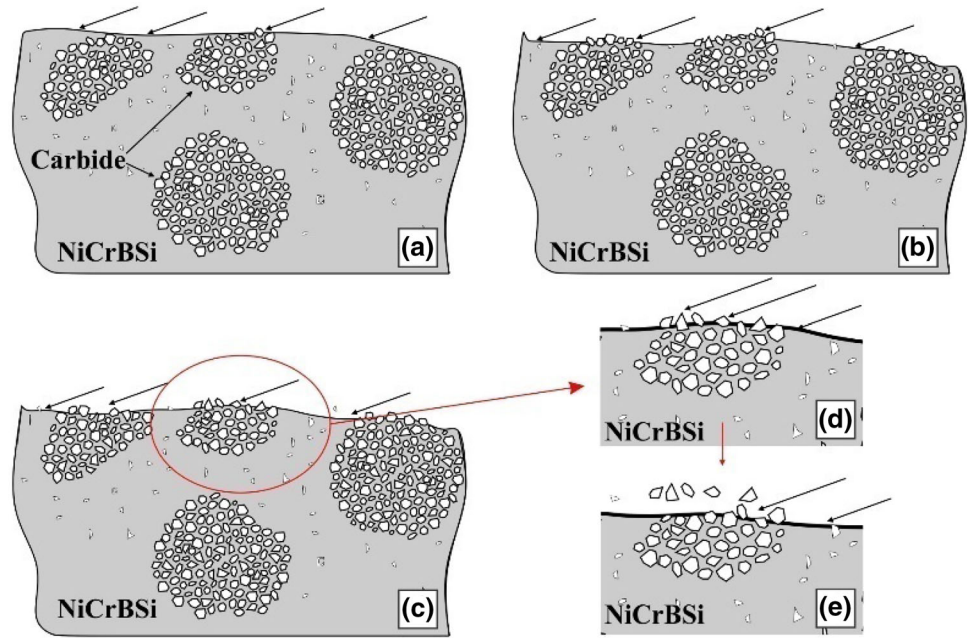
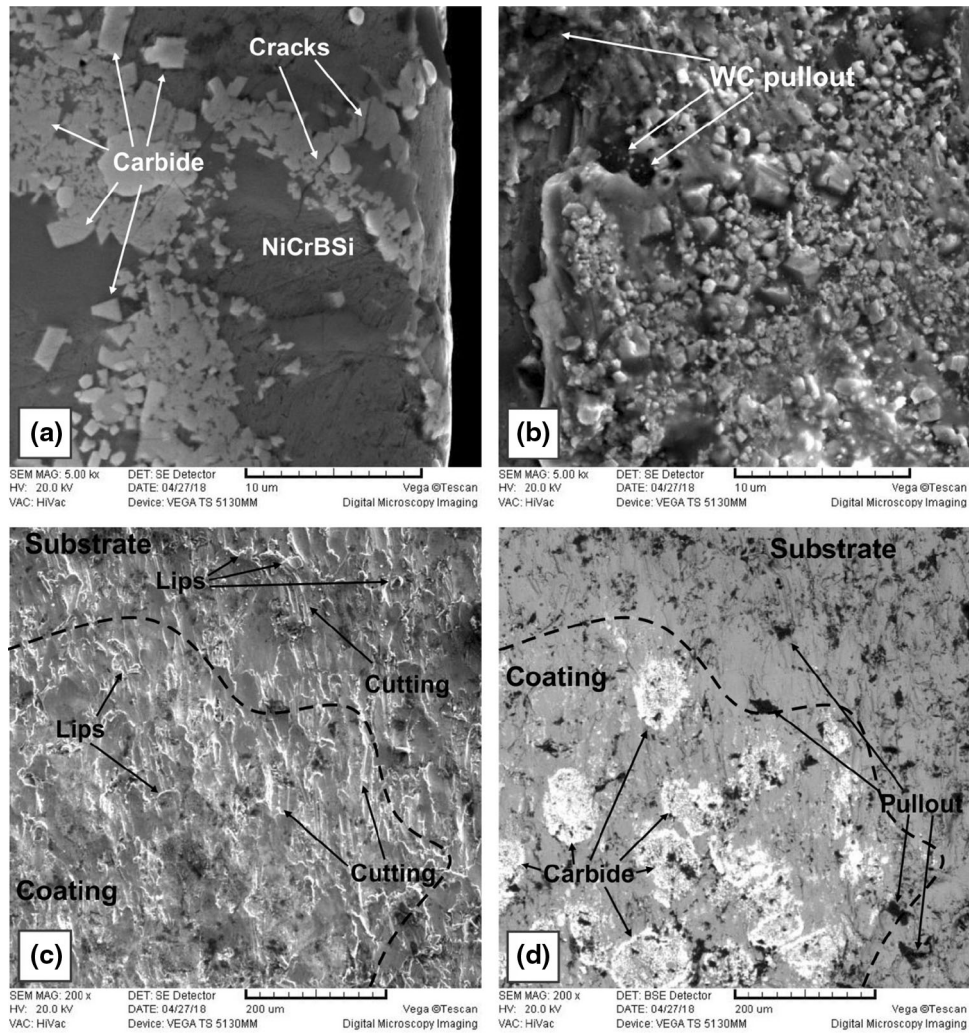


Fig. 11 SEM micrographs showing the eroded surface morphology of WC/NiCrBSi (FS) coating: **a** cross section; **b–d** topographical images



plastic deformation and lips. Only sporadic individual carbides particles are ejected from the surface during the impact of erodent particles.

Acknowledgement This work was financially supported by the Ministry of Education, Science and Technological Development of the Republic of Serbia through the Project No. TR 35024. We would like to express our very great appreciation to Dr Milan Jovanović for his valuable and constructive suggestions during the writing and discussion of this research work. His willingness to give his time so generously has been very much appreciated.

References

- Hutchings I M, *J Phys D: Appl Phys* **25** (1992) A212.
- Nguyen Q B, Nguyen V B, Lim C Y H, Trinh Q T, Sankaranarayanan S, Zhang Y W, Gupta M, *Wear* **321** (2014) 87.
- Tilly G P, in *Treatise on Materials Science and Technology*, (ed) Scott D, *Wear* **13**, Academic Press, New York (1979), p 287.
- Evans A G, in *Treatise on Materials Science and Technology*, (ed) Preece C M, *Materials Erosion* **16**, Academic Press, New York (1979), p 1.
- Andrews D R, Field J E, *J Phys D Appl Phys* **15** (1982) 2357.
- Bousser E, Martin L, Klemberg-Sapieha J E, *J Mater Sci*, **48** (2013) 5543.
- Maasberg J A, Levy A V, *Wear* **73** (1981) 355.
- Gat N, Tabakoff W, *Wear* **50** (1978) 85.
- Sundararajan G, Roy M, *Tribol Int*, **30** (1997) 339.
- López D, Congote J P, Cano J R, Toro A, Tschiptschin A P, *Wear* **259** (2005) 118.
- Islam Md A, Farhat Z N, *Wear* **311** (2014) 180.
- Al-Bukhaiti M A, Ahmed S M, Badran F M F, Emara K M, *Wear* **262** (2007) 1187.
- Manisekaran T, Kamaraj M, Sharrif S M, Joshi S V, *J Mater Eng Perform* **16** (2007) 567.
- Oka Y I, Ohnogi H, Hosokawa T, Matsumura M, *Wear* **203–204** (1997) 573.
- Sugiyama K, Nakahama S, Hattori S, Nakano K, *Wear* **258** (2005) 768.
- Fauchais P L, Heberlein J V R, Boulos M I, *Thermal Spray Fundamentals - From Powder to Part*, Springer, New York (2014).
- Pawlowski L, *The Science Engineering of Thermal Spray Coatings, 2nd ed.*, Wiley, London (2008).
- Fan C, Chen M-C, Chang C-M, Wu W, *Surf Coat Tech* **201** (2006) 908.
- Maslarevic A, Bakic G, Sijacki Zeravcic V, Rajcic B, Lukic U, in Proc of the 3rd IIW South-East European Welding Congress *Welding and joining technologies for a sustainable development and environment*, ISIM Timisoara, Timisoara (2015) p 283.
- Bakić G M, Maksimović V, Maslarević A, Djukić M B, Rajičić B, Djordjević A, in Proc *Metallurgical and Materials Engineering Congress of South-East Europe 2015*, (ed) Korać M, Association of Metallurgical Engineers of Serbia (AMES), Belgrade (2015) p 195.
- Maslarevic A, Lukic U, Bakic G, Martic I, in Proc of the 18th International Research/Expert Conference *Trends in the development of machinery and associated technology*, TMT 2014, Hungary (2014) p 445.
- Mendez P F, Barnes N, Bell K, Borle S D, Gajapathi S S, Guest S D, Izadi H, Gol A K, Wood G, *J Manuf Process* **16** (2014) 4.
- Deuis R L, Yellup J Subramanian M C, *Compos Sci Technol* **58** (1998) 299.
- Ferreira L D S, Graf K, Scheid A, *Mater Res* **18** (2015) 212.
- Drozda F O, Takano H, Oliveira A, *Thermal Spray 2008: Crossing Borders* (DVS-ASM) (2008) p. 757.
- Haugen K, Kvernfold O, Ronold A, Sandberg R, *Wear* **186–187** (1995) 179.
- Badisch E, Kirchgaßner M, *Surf Coat Tech* **202** (2008) 6016.
- Azimi Gh, Shamanian MS, Firozi P, *Int J Surf Sci Eng* **6** (2012) 15.
- Badisch E, Ilo S, Polak R, *Trib Lett* **36** (2009) 55.
- Liyanage T, Fisher G, Gerlich A P, *Wear* **274–275** (2012) 345.
- Katsich C, Badisch E, *Surf Coat Tech* **206** (2011) 1062.
- Sijacki Zeravcic V, Bakic G, Djukic M, Rajcic B, Andjelic B, Parts I and II. Technical Report No 12-04a-12.04/2009, Faculty of Mechanical Engineering, University of Belgrade (2009).
- Finnie I, *Wear* **19** (1972) 81.
- Dallaire S, *J Therm Spray Techn* **10** (2001) 511.
- Maslarević A, Bakić G M, Đukić M B, Rajičić B, Maksimović V, *Hem Ind* **73** (2018) 139.
- Peat T, Galloway A, Toumpis A, Harvey D, Yang W H, *Surf Coat Tech* **300** (2016) 118.
- Vieira R E, Mansouri A, McLaury B S, Shirazi A, *Powder Technol* **288** (2016) 339.
- Cernuschi F, Guardamanga C, Capelli S, Lorenzoni L, Mack D E, Moscatelli A, *Wear* **348–349** (2016) 43.
- Ruff A W, Ives L K, *Wear* **35** (1975) 195.
- Liyanage T, Fisher G, Gerlich A P, *Surf Coat Tech* **205** (2010) 759.
- Chaliampalias D, Vourlias G, Pavlidou E, Skolianos S, Chrissafis K, Stergioudis G, *Applied Surf Sci* **255** (2009) 3605.
- Liu C, Peng H, Zhao Y, Yuan Y, Guo H-B, Xu H-B, *Rare Met.* **38** (2019) 814.
- Guo C, Zhou J, Chen J, Zhao J, Yu Y, Zhou H, *Wear* **270** (2011) 492.
- Wassilkowska A, Czaplicka-Kotas A, Zielina M, Bielski A, Technical Trans, *Chemia Zeszyt 1-ch* **18** (2014) 133.
- Burgess S, Li X, Holland J, *Microscopy and Analysis* **6** (2013) S8.
- Navas C, Colaço R, Damborenea J D, Vilar R, *Surf Coat Tech* **200** (2006) 6854.
- Cockeram B V, *Metal Mater Trans A* **33A** (2002) 33.
- Kalpakjian S, Schmid S R, *Manufacturing Engineering and Technology*, 6th edition, Prentice Hall, 2009.
- Badisch E, Manish R, *Surface Engineering for Enhanced Performance against Wear*, (ed) Manish R, Springer, Wien (2013), p 149.
- Ilo S, Just C, Badisch E, Wosik J, Danninger H, *Mater Sci Eng A* **527** (2010) 6378.
- Jones M, Waag U, *Wear* **271** (2011) 1314.
- Just Ch, Badisch E, Wosik J, *J Mater Process Tech* **210** (2010) 408.
- Kim H-J, Hwang S-Y, Lee C-H, Juvanon P, *Surf Coat Tech* **172** (2003) 262.
- Tu J, Liu M S, Mao Z Y, *Wear* **209** (1997) 43.
- González R, Cadenas M, Fernández R, Cortizo J L, Rodríguez E, *Wear* **262** (2007) 301.
- Braunovic M, Sijacki Zeravcic V, Bakic G, Djukic M, Markovic D, *Boiler Tube Erosion in Thermal Power Plants*, CEA Technologies Inc; (2006) CEATI Project and Report No: T052700-0122.
- Rodríguez J, Martin A, Fernández R, Fernández JE, *Wear* **255** (2003) 950.

Publisher's Note Springer Nature remains neutral with regard to jurisdictional claims in published maps and institutional affiliations.